Free planar isotropic-nematic interfaces in binary hard-rod fluids

Kostya Shundyak and René van Roij
Institute for Theoretical Physics, Utrecht University, Leuvenlaan 4, 3584 CE Utrecht, The Netherlands
(Received 20 August 2003; published 18 December 2003)

Within the Onsager theory we study free planar isotropic-nematic interfaces in binary mixtures of hard rods. For sufficiently different particle shapes the bulk phase diagrams of these mixtures exhibit a triple point, where an isotropic (I) phase coexists with two nematic phases (N_1 and N_2) of different composition. For all explored mixtures we find that upon approach of the triple point the I-N_2 interface shows complete wetting by an intervening N_1 film. We compute the surface tensions of isotropic-nematic interfaces, and find a remarkable increase with fractionation, similar to the effect in polydisperse hard-rod fluids.

DOI: 10.1103/PhysRevE.68.061703 PACS number(s): 61.30.Hn, 05.70.Np, 68.03.Cd, 68.08.Bc

I. INTRODUCTION

Colloidal suspensions of rodlike particles are well known to exhibit a wealthy phase behavior as a function of density [1–3]. Early experiments on vanadiumpentoxide solutions [4] and suspensions of tobacco mosaic virus (TMV) particles [5] showed a first-order transition from a disordered (isotropic) fluid phase to an ordered (liquid-crystalline nematic) fluid phase upon increasing the concentration of rods sufficiently. The nematic is homogeneous (it is a fluid), but the rods are on average oriented in a specific direction $\hat{\boldsymbol{n}}$, the so-called nematic director. The bulk nematic ordering is of uniaxial symmetry, i.e., there is azimuthal symmetry about $\hat{\boldsymbol{n}}$. The isotropic-nematic (I-N) transition was first explained by Onsager, who modeled the colloidal rods as hard needles. He first showed that the average pairwise excluded volume is reduced in the nematic phase compared to the isotropic phase, and then argued that the resulting gain of free volume (and hence translational entropy) compensates the loss of orientation entropy (due to the nematic ordering) at sufficiently high concentrations of rods [6]. In other words, the ordering follows as a consequence of maximizing the total entropy. More recently it was shown that a further increase of the concentration of TMV can also give rise to smectic ordering [7,8], where the translational invariance is broken and the system forms a layered structure. In the 1980s and 1990s computer simulations [9,10], and later density functional theories [11–13], have shown that also the smectic phase can be explained by the hard-rod model for colloidal rods. One concludes, therefore, that the bulk phase behavior of these systems is well understood by now.

Onsager's theory for hard rods has been extended to describe bulk *mixtures* of colloidal rods. For the case of binary mixtures of longer and shorter rods, it was found that the I-N transition is accompanied by strong fractionation, such that the coexisting nematic phase contains a relatively large fraction of the longer rods [14,15]. Later theoretical work on long-short mixtures also showed the possibility of nematic-nematic (N_1-N_2) demixing (driven by a peculiar competition between orientation entropy and ideal mixing entropy), and an isotropic-nematic-nematic (I-N_1-N_2) triple point in the phase diagram [16–19] of mixtures with a length ratio more extreme than about 1:3. Later also binary mixtures of thin and thick hard rods were considered. They were shown to have phase diagrams similar to those of long-short mixtures, i.e., with strong fractionation at I-N coexistence and with N_1-N_2 and I-N_1-N_2 coexistence for diameter ratios exceeding 1:3.8 [18–21], but with an additional possibility for isotropic-isotropic (I_1-I_2) phase coexistence due to the depletion effect [20–22] if the diameter ratio is more extreme than about 1:8. Interestingly, thin-thick mixtures have recently been realized experimentally by mixing "bare" fd virus particles (length 1 μm) with ones that are "coated" with polyethyleneglycol (PEG) [23]. The diameter ratio of these systems can be tuned by varying the ionic strength of the solvent: due to an increasing salt concentration the effective diameter of the (charged) bare rods shrinks because of enhanced screening, whereas that of the PEG-coated rods is not (or hardly) affected because of the steric nature of PEG. Exploiting this effect allowed for the experimental study of diameter ratios up to about 1:4.5, and I-N_1, I-N_2, N_1-N_2 as well as I-N_1-N_2 triple coexistence were actually observed [23].

The present study is devoted to the planar interfaces that exist between the coexisting bulk phases in binary mixtures of colloidal rods. Our focus is on the calculation of both thermodynamic and structural properties of these interfaces. The main thermodynamic quantity of interest is the surface tension γ, and the structural properties we will investigate are the profiles of the density and the order parameters. It is known from the study of the I-N interface of pure (one-component) suspensions of rods that γ depends on the angle between the interface normal $\hat{\boldsymbol{z}}$ and the director $\hat{\boldsymbol{n}}$ of the nematic phase asymptotically far from the interface [24–26]. The study of Refs. [24,27] showed that γ is minimal when $\hat{\boldsymbol{n}} \perp \hat{\boldsymbol{z}}$, and on this basis (and on the basis of some of our own test calculations) we assume this to be the case for mixtures as well. It is also established by now [24,27,28] that (i) the density profile and the nematic order parameter profile of the I-N interface of the pure hard needle fluid change monotonically from their values in the isotropic bulk phase to those in the nematic phase, (ii) the interface thickness is of the order of the length L of the rods, and (iii) the interfacial biaxiality is small and nonmonotonic. In this paper we will show that the density profiles in mixtures of rods are *not* always monotonic, and that the interface thickness not always of order L

due to the formation of macroscopically thick wetting films close to the bulk triple points. Some of these findings have been reported briefly elsewhere [30]. Moreover, we will show that the tension in mixtures of rods tends to be substantially higher than that of the pure systems of their components.

This paper is organized as follows. In Sec. II we introduce the Onsager functional and the basic Euler-Lagrange equation. In Sec. III we solve this equation for bulk geometries, and we present a few typical bulk phase diagrams. In Sec. IV we present our method to solve the Euler-Lagrange equation for interface geometries, and study I-N_1, N_1-N_2 and I-N_2 interfaces, the latter in particular in the vicinity of the bulk I-N_1-N_2 triple point. A summary and some discussion of our results will be presented in Sec. V.

II. DENSITY FUNCTIONAL

We consider a fluid of hard cylinders of two different species $\sigma=1,2$ of length L_σ and diameter D_σ in a macroscopic volume V at temperature T and chemical potentials μ_σ. The thermodynamic properties and the structure of the system can be determined from the grand potential functional $\Omega[\{\rho_\sigma\}]$ of the one-particle distribution functions $\rho_\sigma(\boldsymbol{r},\hat{\boldsymbol{\omega}})$, where $\boldsymbol{r}$ denotes the center-of-mass coordinate of the rod of species σ and $\hat{\boldsymbol{\omega}}$ the orientation of the long axis. The functional $\Omega[\{\rho_\sigma\}]$ is such that (i) it is minimized, for given $(\{\mu_\sigma\},V,T)$, by the equilibrium one-particle distributions $\rho_\sigma(\boldsymbol{r},\hat{\boldsymbol{\omega}})$, and (ii) the minimal value of the functional is the equilibrium grand potential Ω [31].

Within the second virial approximation and in the absence of external potentials, the functional $\Omega[\{\rho_\sigma\}]$ can be written [1,6] as

$$\beta\Omega[\{\rho_\sigma\}]=\sum_\sigma \int dq\rho_\sigma(q)(\ln[\rho_\sigma(q)L_\sigma^2D_\sigma]-1-\beta\mu_\sigma) - \frac{1}{2}\sum_{\sigma\sigma'}\int dqdq' f_{\sigma\sigma'}(q;q')\rho_\sigma(q)\rho_{\sigma'}(q'), \tag{1}$$

with $\beta=(kT)^{-1}$ the inverse temperature and $f_{\sigma\sigma'}(q;q')$ the Mayer function of the $\sigma\sigma'$ pair of rods with coordinates $q=\{\boldsymbol{r},\hat{\boldsymbol{\omega}}\}$ and $q'=\{\boldsymbol{r}',\hat{\boldsymbol{\omega}}'\}$. For hard rods, the focus of our study, $f_{\sigma\sigma'}(q;q')$ equals -1 if the rods overlap and vanishes otherwise. Onsager argued that the second virial approximation is accurate for long rods, and becomes even exact for isotropic and nematic bulk fluids in the limit of vanishing diameter-to-length ratio [6]. We shall adopt this limit throughout this paper, i.e., we consider $D_\sigma/L_{\sigma'}\to 0$ for any $\sigma\sigma'$ pair. Therefore, the relative shape of the rods is only characterized by the ratios $l=L_2/L_1$ and $d=D_2/D_1$ of the lengths and the diameters, respectively.

The minimum conditions $\delta\Omega[\{\rho_\sigma\}]/\delta\rho_\sigma(q)=0$ on the functional lead to the set of nonlinear integral equations

$$\ln[\rho_\sigma(q)L_\sigma^2D_\sigma]-\sum_{\sigma'}\int dq' f_{\sigma\sigma'}(q;q')\rho_{\sigma'}(q')=\beta\mu_\sigma \tag{2}$$

to be solved for the equilibrium distributions $\rho_\sigma(q)$. Once determined, they can be inserted into the functional to obtain the equilibrium value of the grand potential

$$\beta\Omega=\frac{1}{2}\sum_\sigma\int dq\rho_\sigma(q)(\ln[\rho_\sigma(q)L_\sigma^2D_\sigma]-2-\beta\mu_\sigma). \tag{3}$$

Note that $\Omega=-pV$ for a bulk system in a volume V, with $p=p(\{\mu_\sigma\},T)$ the pressure. In the presence of a planar surface or interface of area A we have $\Omega=-pV+\gamma A$ with $\gamma=\gamma(\{\mu_\sigma\},T)$ the surface or interface tension.

In general, fluctuations of the interface position (capillary waves) are important in the analysis of fluid-fluid interfaces. The amplitude of such fluctuations is controlled by the ''wetting parameter'' [32,33]

$$\omega\equiv\frac{k_BT}{4\pi\gamma\xi^2}, \tag{4}$$

where ξ is the bulk correlation length. For rods of typical length L and diameter D we shall see that $\xi\sim L$ and $\gamma\sim k_BT/LD$, and hence $\omega\sim D/L$, i.e., ω vanishes in the Onsager limit. As a consequence the capillary-wave fluctuations are unimportant, i.e., the mean-field density functional (1) is sufficient to describe interfacial phenomena in fluids of long hard rods.

III. BULK PHASE DIAGRAMS

The bulk thermodynamic properties of binary hard-rod fluids were studied extensively within Onsager theory. The minimization of the functional was either performed variationally [16–19,22,34] or through a fully numerical solution [14,21,28]. We adopted the latter approach as it can be easily generalized for inhomogeneous systems. For clarity we briefly repeat the essential points of the method and summarize the available results.

The bulk distribution functions of the isotropic and nematic phase are translationally invariant, i.e., $\rho_\sigma(\boldsymbol{r},\hat{\boldsymbol{\omega}})=\rho_\sigma(\hat{\boldsymbol{\omega}})$, which allows us to reduce Eq. (2) to

$$\ln[\rho_\sigma(\hat{\boldsymbol{\omega}})L_\sigma^2D_\sigma]+\sum_{\sigma'}\int d\hat{\boldsymbol{\omega}}' E_{\sigma\sigma'}(\hat{\boldsymbol{\omega}},\hat{\boldsymbol{\omega}}')\rho_{\sigma'}(\hat{\boldsymbol{\omega}}')=\beta\mu_\sigma, \tag{5}$$

with $E_{\sigma\sigma'}$ the excluded volume of a pair of cylinders of species σ and σ' given by [1]

$$E_{\sigma\sigma'}(\hat{\boldsymbol{\omega}},\hat{\boldsymbol{\omega}}')=-\int d\boldsymbol{r}' f_{\sigma\sigma'}(\boldsymbol{r},\hat{\boldsymbol{\omega}};\boldsymbol{r}',\hat{\boldsymbol{\omega}}') = L_\sigma L_{\sigma'}(D_\sigma+D_{\sigma'})|\sin\gamma| \tag{6}$$

in terms of the angle γ between $\hat{\boldsymbol{\omega}}$ and $\hat{\boldsymbol{\omega}}'$, i.e., $\gamma = \arccos(\hat{\boldsymbol{\omega}}\cdot\hat{\boldsymbol{\omega}}')$. Note that additional $O(LD^2)$ terms are being ignored in Eq. (5), in line with the needle limit $(D_\sigma/L_{\sigma'}\to 0)$ of interest here.

At sufficiently low $\{\beta\mu_\sigma\}$ the only stable solution of Eq. (5) is the isotropic distribution $\rho_\sigma^I(\hat{\boldsymbol{\omega}})=n_\sigma/(4\pi)$, with $n_\sigma = \int d\hat{\boldsymbol{\omega}}\rho_\sigma(\hat{\boldsymbol{\omega}})$ the bulk number density of species σ. As μ_σ are high enough, one or, possibly, two sets of stable uniaxial solutions $\rho_\sigma^N(\hat{\boldsymbol{\omega}})=\rho_\sigma(\theta)$ exist, with $\theta=\arccos(\hat{\boldsymbol{\omega}}\cdot\hat{\boldsymbol{n}})$ the angle between $\hat{\boldsymbol{\omega}}$ and the nematic director $\hat{\boldsymbol{n}}$. These distributions have "up-down" symmetry, $\rho_\sigma(\theta)=\rho_\sigma(\pi-\theta)$, hence $\rho_\sigma(\theta)$ needs only to be determined for $\theta\in[0,\pi/2]$. Using an equidistant θ-grid of $N_\theta=30$ points $\theta_i\in[0,\pi/2]$, where $1\leqslant i\leqslant N_\theta$, we iteratively solve Eq. (5) for the set of $2N_\theta$ equations in order to find $\rho_\sigma(\theta_i)$ numerically. The integral in Eq. (5) is calculated with the trapezoidal rule. Coexistence of different phases $\{I,N_1,N_2\}$ can be determined by imposing conditions of mechanical and chemical equilibrium.

In order to gauge the accuracy of the chosen θ-grid we calculate the resulting densities of the coexisting isotropic and nematic phase of the one-component system. We find $n^IL^2D(\pi/4)=3.281\pm0.001$, $n^NL^2D(\pi/4)=4.172\pm0.001$; the nematic order parameters of the two coexisting phases are $S^I=0.008\pm0.001$ and $S^N=0.791\pm0.001$, and the pressure $(\pi/4)\beta pL^2D=14.045\pm0.001$. These data, based on $N_\theta=30$, differ by less then a percent from the most accurate results available in the literature [1], which we can reproduce with $N_\theta\geqslant 80$. In order to have consistency between bulk and interfacial results we take $N_\theta=30$ in most of our calculations. The exception is the case of long-short mixtures in the nematic phase, which requires $N_\theta=50$ for acceptable accuracy.

In Fig. 1 we show both pressure-composition (a) and density-density (b) representations of bulk phase diagrams of thin-thick binary mixtures $(L_\sigma=L, D_2>D_1)$ for several diameter ratios $d\equiv D_2/D_1$. In Fig. 1(a) the composition variable $x=n_2/(n_1+n_2)$ denotes the mole fraction of thick rods and $f=(p-p_{thick})/(p_{thin}-p_{thick})$ is a dimensionless shifted pressure which takes the values $f=1,0$ at isotropic-nematic coexistence of the pure-thin $(x=0)$ and pure-thick $(x=1)$ systems, respectively. Note that $(\pi/4)\beta p_{thin}L^2D_1=(\pi/4)\beta p_{thick}L^2D_2=14.045$, i.e., $p_{thick}=p_{thin}/d$, and that the tie lines connecting coexisting phases are horizontal in the f-x representation of Fig. 1(a).

At low pressures (or low densities) the phase diagrams show an isotropic (I) phase and at higher pressures (or densities) one ($d=3.0,3.5$) or two ($d=4.0,4.2$) nematic phases (N_1 and N_2). For diameter ratios $d=3.0,3.5$ the phase diagram is spindlelike, and the only feature is a strong fractionation at coexistence, such that the nematic phase is relatively rich in thick rods and the isotropic phase in thin ones. The reason behind this fractionation is the relatively large excluded volume in interactions of the thick rods, which makes them more susceptible to orientational ordering [14,19,21]. The fractionation of isotropic-nematic coexistence becomes stronger for increasing d. For $3.8<d<4.29$ the bulk phase diagram develops nematic-nematic (N_1-N_2) coexistence in a pressure regime $p_t<p<p_c$, with p_t the triple-point pressure

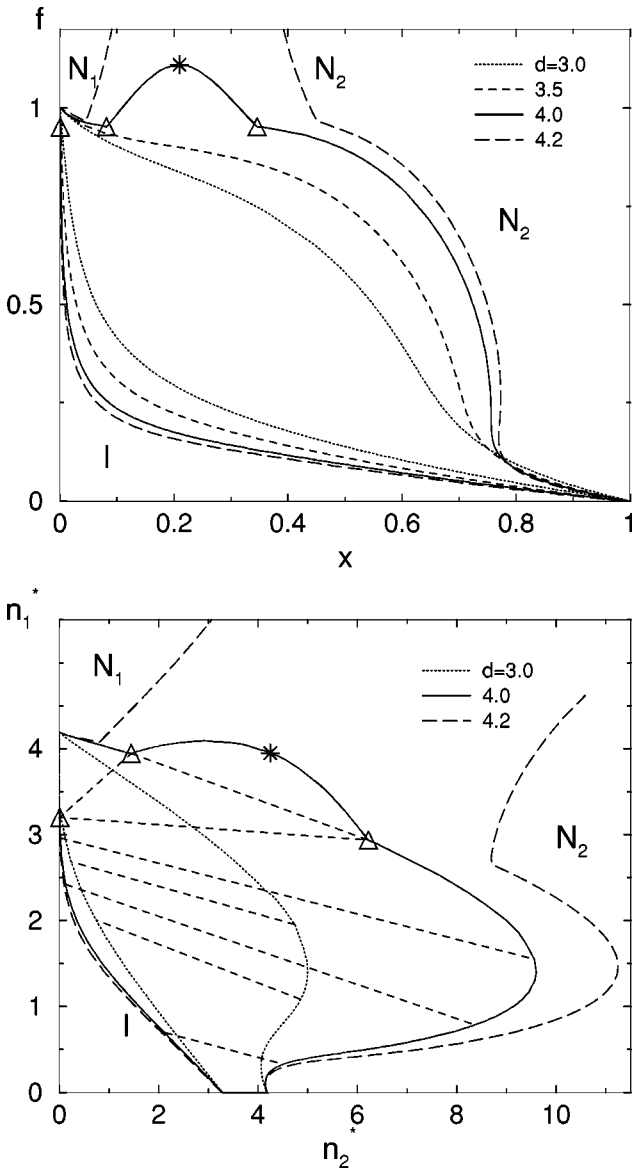

FIG. 1. (a) Bulk phase diagrams of binary thin-thick mixtures for different diameter ratios d in the f-x representation, with $f=(p-p_{thick})/(p_{thin}-p_{thick})$ the dimensionless shifted pressure, and x the mole fraction of the thicker rods. We distinguish the fully symmetric isotropic phase (I) and orientationally ordered nematic phases (N_1 and N_2). For the diameter ratio $d=4.0$ the I-N_1-N_2 triple phase coexistence is marked by ($\triangle$), and the N_1-N_2 critical point by (*). (b) The same phase diagrams in density-density representation, where $n_1^*=n_1LD_1^2(\pi/4)$ and $n_2^*=n_2LD_2^2(\pi/4)$ are the dimensionless bulk number densities of thin and thick rods, respectively. The tie lines connect coexisting state points.

and p_c the critical (consolute) pressure. For $d=4.0$ the consolute point is indicated by (*) in Fig. 1. The mechanism of this demixing transition was spelled out in detail in Refs. [17,21], and involves a competition between orientational entropy (favoring demixing) and entropy of mixing (favoring mixing). Interestingly, the width of fractionation gap $\Delta x = x_{N_1}-x_{N_2}$ for the triple point N_1 and N_2 phases scales linearly with the triple-point pressure p_t. The critical pressure

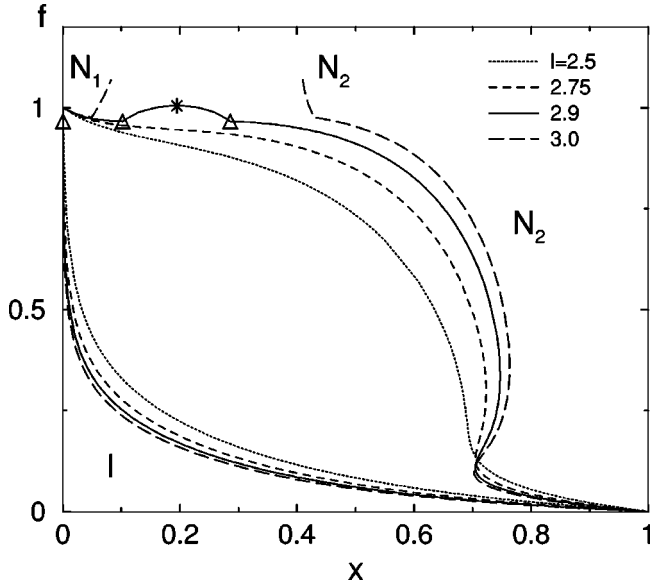

FIG. 2. Bulk phase diagrams of binary long-short mixtures for different length ratio l in the f-x representation (see caption to Fig. 1). (△) mark I-N_1-N_2 triple phase coexistence and (*) marks N_1-N_2 critical point for $l=3.0$.

of the N_1-N_2 transition diverges as $d\rightarrow 4.29$ [17,21]. For $d>3.8$ the lower bound of the N_1-N_2 coexistence is an I-N_1-N_2 triple point, indicated by triangles (△) in Fig. 1 for $d=4.0$. With increasing d the triple point I and N_1 phases approach the pure-thin bulk coexistence (i.e., $x_{I,N_1}\rightarrow 0$), whereas the composition of the triple point N_2 phase shifts to a pure-thick phase ($x_{N_2}\rightarrow 1$).

The f-x representation is convenient for our analysis, whereas the densities (volume fractions) of thin and thick rods are experimental control parameters [3]. For this reason the same phase diagrams of thin-thick binary mixtures are shown in Fig. 1(b) in density-density representation, with $n_1^*=n_1LD_1^2(\pi/4)$ and $n_2^*=n_1LD_2^2(\pi/4)$ being the dimensionless bulk number densities of thin and thick rods, respectively. In this representation the tie lines are no longer horizontal.

In Fig. 2 a set of bulk phase diagrams for long-short binary mixtures ($D_\sigma=D, L_2>L_1$) for several length ratios $l\equiv L_2/L_1$ is presented. Here $x=n_2/(n_1+n_2)$ denotes the fraction of long rods and $f=(p-p_{long})/(p_{short}-p_{long})$ with $p_{long}=p_{short}/l^2$. All characteristic features of the phase diagrams are the same as in thin-thick mixtures. The fractionation of the coexisting I-N_2 and N_1-N_2 phases has a strong dependence on l, and limits the values accessible for calculations to $l\leqslant 3.1$ for the chosen grids and the required accuracy. The main reason is that the nematic ordering in the triple-point N_2 phase is very pronounced, requiring a fine grid [21].

IV. FREE INTERFACES

We now turn to the thermodynamics and the structure of the free interfaces between the coexisting phases. We assume that the interfaces are planar, with surface normal $\hat{z}$. The nematic director $\hat{n}$ of the asymptotic nematic bulk phase(s) can, in general, have a nontrivial tilt angle $\theta_t=\arccos(\hat{\boldsymbol{n}}\cdot\hat{\boldsymbol{z}})$ with respect to the interface normal. In the present calculations we restrict attention to $\theta_t=\pi/2$, i.e., $\hat{\boldsymbol{n}}\perp\hat{\boldsymbol{z}}$. This geometry is known to be thermodynamically favorable because of its minimal surface tension [24,29].

The equilibrium distribution functions $\rho_\sigma(z,\hat{\boldsymbol{\omega}})$ depend on the spatial coordinate $z=\hat{\boldsymbol{z}}\cdot\boldsymbol{r}$, and angular coordinates $\hat{\boldsymbol{\omega}}=(\theta,\varphi)$ defined by $\cos\theta=\hat{\boldsymbol{n}}\cdot\hat{\boldsymbol{\omega}}$ and $\sin\theta\sin\varphi=\hat{\boldsymbol{z}}\cdot\hat{\boldsymbol{\omega}}$. These functions are solutions of the Euler-Lagrange equations Eq. (2) at the coexisting chemical potentials $\beta\mu_\sigma=\beta\mu_\sigma^{coex}$, with boundary conditions $\rho_\sigma(z\rightarrow\pm\infty,\hat{\boldsymbol{\omega}})=\rho_\sigma^{(\pm)}(\theta)$ being the two coexisting bulk distributions [labeled by $(+)$ and $(-)$ here for brevity].

The planar symmetry, i.e., the independence of $\rho_\sigma(z,\hat{\boldsymbol{\omega}})$ of the in-plane coordinates x and y, allows for a reduction of the numerics, since the "excluded slab" $\mathcal{K}_{\sigma\sigma'}(z,\hat{\boldsymbol{\omega}},z',\hat{\boldsymbol{\omega}}')=-\int dx'dy' f_{\sigma\sigma'}(\boldsymbol{r},\hat{\boldsymbol{\omega}};\boldsymbol{r}',\hat{\boldsymbol{\omega}}')$ can be calculated analytically [25,28]. This reduces the Euler-Lagrange equations to

$$\beta\mu_\sigma^{coex}=\ln[\rho_\sigma(z,\hat{\boldsymbol{\omega}})L_\sigma^2D_\sigma]+\sum_{\sigma'}\int dz'\int d\hat{\boldsymbol{\omega}}'\times\mathcal{K}_{\sigma\sigma'}(|z-z'|,\hat{\boldsymbol{\omega}},\hat{\boldsymbol{\omega}}')\rho_{\sigma'}(z',\hat{\boldsymbol{\omega}}'),\qquad(7)$$

where the expression for $\mathcal{K}_{\sigma\sigma'}(|z|,\hat{\boldsymbol{\omega}},\hat{\boldsymbol{\omega}}')$ is given in the Appendix.

In principle one could now solve Eq. (7) on a (z,θ,φ) grid. However, the numerical efforts can be further reduced if one realizes that biaxiality, i.e., the φ dependence, is weak [27,28]. In that case the truncated expansion

$$\rho_\sigma(z,\theta,\varphi)=\sum_{m=0}^{M}\rho_{\sigma,m}(z,\theta)\cos(2m\varphi)\qquad(8)$$

is expected to be accurate for small M, and hence only a few "coefficients" $\rho_{\sigma,m}(z,\theta)$ $(m\leqslant M)$ need to be determined on a (z,θ) grid. It is important to realize, however, that Eq. (8) implicitly assumes that the nematic director $\hat{\boldsymbol{n}}$ does not vary in space. The coefficients $\rho_{\sigma,m}(z,\theta)$ follow from an insertion of Eq. (8) into Eq. (7), multiplication by $\cos(2m\varphi)$, and integration over φ $(0\leqslant\varphi\leqslant 2\pi)$. For $M=0$ this yields

$$\beta\mu_\sigma^{coex}=\ln[\rho_{\sigma,0}(z,\theta)L_\sigma^2D_\sigma]+\sum_{\sigma'}\int dz'd\theta'\sin\theta'\times\mathcal{K}_{\sigma\sigma'}^{00}(z-z',\theta,\theta')\rho_{\sigma',0}(z',\theta'),\qquad(9)$$

where $\mathcal{K}_{\sigma\sigma'}^{00}(z-z',\theta,\theta')=(2\pi)^{-1}\int_0^{2\pi}\int_0^{2\pi}d\varphi d\varphi'\mathcal{K}_{\sigma\sigma'}(z-z',\hat{\boldsymbol{\omega}},\hat{\boldsymbol{\omega}}')$ is the doubly azimuthally integrated excluded slab, which we determine numerically once on an appropriate grid.

The lowest-order correction that takes into account biaxiality results from $M=1$, and yields $\rho_{\sigma,m}(z,\theta)$, $(m=0,1)$ from the coupled set of equations

$$\beta\mu_\sigma^{coex}=\ln[\rho_{\sigma,0}(z,\theta)L_\sigma^2 D_\sigma]+I_0\left(\frac{\rho_{\sigma,1}(z,\theta)}{\rho_{\sigma,0}(z,\theta)}\right)$$
$$+\sum_{\sigma'}\int dz'\,d\theta'\sin\theta'(\mathcal{K}^{00}_{\sigma\sigma'}(z-z',\theta,\theta')$$
$$\times\rho_{\sigma',0}(z',\theta')+\mathcal{K}^{01}_{\sigma\sigma'}(z-z',\theta,\theta')$$
$$\times\rho_{\sigma',1}(z',\theta')),$$
$$0=I_1\left(\frac{\rho_{\sigma,1}(z,\theta)}{\rho_{\sigma,0}(z,\theta)}\right)+\sum_{\sigma'}\int dz'\,d\theta'\sin\theta'$$
$$\times(\mathcal{K}^{10}_{\sigma\sigma'}(z-z',\theta,\theta')\rho_{\sigma',0}(z',\theta')$$
$$+\mathcal{K}^{11}_{\sigma\sigma'}(z-z',\theta,\theta')\rho_{\sigma',1}(z',\theta')),\qquad(10)$$

with $\mathcal{K}^{km}_{\sigma\sigma'}(z-z',\theta,\theta')=(2\pi)^{-1}\int_0^{2\pi}\int_0^{2\pi}d\varphi\,d\varphi'\cos(2k\varphi)\times\cos(2m\varphi')\mathcal{K}_{\sigma\sigma'}(z-z',\hat{\boldsymbol{\omega}},\hat{\boldsymbol{\omega}}')$, $k,m=\{0,1\}$, again to be determined numerically only once, with

$$I_0(x)=\frac{1}{2\pi}\int_0^{2\pi}d\varphi\,\ln[1+x\cos(2\varphi)]=\ln\frac{1+\sqrt{1-x^2}}{2},$$

$$I_1(x)=\frac{1}{2\pi}\int_0^{2\pi}d\varphi\cos(2\varphi)\ln[1+x\cos(2\varphi)]$$
$$=\frac{1-\sqrt{1-x^2}}{x},$$

for $|x|<1$.

Note that the boundary conditions imply that $\rho_{\sigma,1}(z,\theta)\to 0$ for $|z|\to\infty$. In general, the solutions $\rho_{\sigma,0}(z,\theta)$ for $M=0$ are not identical to $\rho_{\sigma,0}(z,\theta)$ for $M=1$, but the difference is small in most cases since $|\rho_{\sigma,1}(z,\theta)L_\sigma D_\sigma^2|\ll 1$. In the remainder of this paper we shall mainly concentrate on solutions of Eq. (9), although some results of Eqs. (10) will be discussed.

By iteration of Eq. (9) [or Eqs. (10)] with the appropriate boundary conditions we calculated $\rho_{\sigma,0}(z,\theta)$ [and $\rho_{\sigma,1}(z,\theta)$] for a number of state points μ_σ^{coex} on the I-N_1, I-N_2 and N_1-N_2 binodals. We used an equidistant spatial grid of $N_z=200$ points $z_i\in[-5L,5L]$, an equidistant angular grid of $N_\theta=30$ points $\theta_j\in[0,\pi/2]$ for thin-thick mixtures or an angular grid of $N_\theta=50$ points $\theta_j\in[0,\pi/2]$ for long-short mixtures. From the equilibrium distributions $\rho_{\sigma,0}(z,\theta)$ we calculated the local density and the nematic order parameter profiles

$$n_\sigma(z)=4\pi\int_0^{\pi/2}d\theta\sin\theta\rho_{\sigma,0}(z,\theta),$$

$$S_\sigma(z)=4\pi\int_0^{\pi/2}d\theta\sin\theta P_2(\cos\theta)\rho_{\sigma,0}(z,\theta)/n_\sigma(z),$$

with $P_2(x)=(3x^2-1)/2$ the second Legendre polynomial. In the case of iterating Eqs. (10) the biaxiality is defined as [27,28]

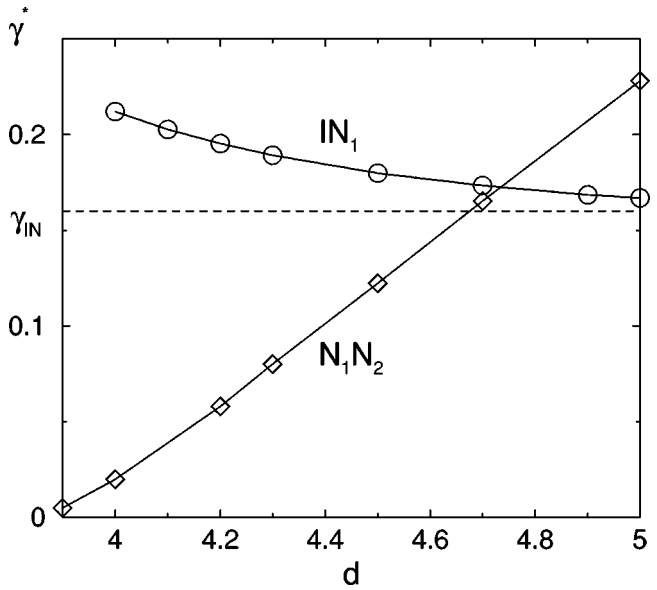

FIG. 3. Dimensionless surface tension $\gamma^*=\beta\gamma/LD_1$ of I-N_1 (○) and N_1-N_2 (◇) interfaces at triple phase coexistence ($p=p_t$) for different diameter ratio d of thin-thick mixtures. The dashed line corresponds to the surface tension of the one-component I-N interface for which $\gamma^*_{I\text{-}N}=0.156\pm0.001$ [28].

$$\Delta_\sigma(z)=\left\langle\frac{3}{2}\sin^2\theta\cos 2\varphi\right\rangle_\sigma=\frac{3}{4n_\sigma(z)}\int_0^{\pi/2}d\theta\sin^3\theta\rho_{\sigma,1}(z,\theta).$$

The interface thickness t is defined as $t=|z_+-z_-|$ where $z_\pm$ are solutions of $n_1'''(z)=0$, where a prime denotes differentiation with respect to z. As this equation has a set of solutions in every interfacial region, we choose ($z_\pm$) be the outermost ones, i.e., the nearest to the bulk phases. This criterion provides a single measure for the thickness of both monotonic and nonmonotonic profiles, with and without a thick film in between the asymptotic bulk phases at $z\to\pm\infty$. Also thin (or short) rods have a smaller excluded volume and a nonvanishing concentration in both coexisting phases, so their density is a convenient representation of structural changes within the interface. The interfacial width for the one-component I-N interface is, with the present definition, given by $t/L=0.697$. We have checked that other definitions of the thickness lead to similar results.

A. I-N_1 and N_1-N_2 interfaces

The I-N_1 interfaces exist only in a small pressure regime $p_{thin}\geqslant p\geqslant p_t$. They closely resemble the I-N interface of the pure hard-rod fluid, i.e., the profiles of the order parameters $S_\sigma(z)$ and the densities $n_\sigma(z)$ change monotonically from the bulk values in the I phase to those in the N_1 phase.

The thickness of the I-N_1 interface is of order L which is similar to that of the pure system. With increasing d the I-N_1 surface tension at triple phase coexistence ($p=p_t$) decreases monotonically to the I-N surface tension of the pure system, as shown in Fig. 3, where the dimensionless surface tension $\gamma^*=\beta\gamma/LD_1$ is plotted. This is expected from an inspection of the phase diagrams as $x_{I,N_1}\to 0$ for increasing d. For the

diameter ratio $d=4.0$ the surface tension at $p=p_t$ is given by $\gamma^*_{I\text{-}N_1}=0.209\pm0.001$ with the same level of accuracy for all other calculations of the surface tensions. For the long-short mixtures the behavior of the surface tension at the I-N_1 interface as a function of length ratio l is very similar. For $l=3.0$ the surface tension at $p=p_t$ is given by $\gamma^*_{I\text{-}N_1}=0.212\pm0.001$.

In general, the order parameter and density profiles are shifted with respect to each other. Such a shift can be characterized by the distance $\delta=|z_n-z_S|$ between the centers z_n and z_S of the density and order parameter profiles, defined by [24]

$$n(z_n)=n_-+\frac{1}{2}(n_+-n_-),$$

$$S(z_S)=S_-+\frac{1}{2}(S_+-S_-),$$

where $+/-$ indicate asymptotic bulk values. A nonzero shift δ reflects the fact that the thickness of the interface is different for rods of different orientations. For monodisperse rods it was found that $\delta=0.50L$ [24]. For binary mixtures δ can be determined for each component separately. For thin-thick mixtures with $d=4.0$ the I-N_1 interface at triple phase coexistence shows $\delta_{thin}=0.35L$ and $\delta_{thick}=0.55L$. For long-short mixtures with $l=3.0$ the effect is similar for the short rods ($\delta_{short}=0.37L_1$) and much more pronounced for the long rods ($\delta_{long}=1.54L_1$, i.e., $\delta_{long}\simeq0.51L_2$).

The profiles of $S_\sigma(z)$ and $n_\sigma(z)$ at N_1-N_2 interfaces are also monotonic. For the diameter ratio $d=4.0$ at $p=p_t$ the interface thickness is given by $t/L=0.592$ and the surface tension $\gamma^*_{N_1\text{-}N_2}=0.019\pm0.001$, which is an order of magnitude smaller than $\gamma^*_{I\text{-}N_1}$. Upon the approach of the critical point $t/L\to\infty$ and the surface tension vanishes. For $d>4.0$ surface tension $\gamma^*_{N_1\text{-}N_2}$ (at $p=p_t$) increases approximately linearly with d as shown in Fig. 3.

The biaxiality is found to be small in both the I-N_1 and the N_1-N_2 interfaces. In Fig. 4 we present the profiles $\Delta_\sigma(z)$ of the triple point I-N_1 and N_1-N_2 (inset) interfaces of the thin-thick mixture with $d=4.0$, as well as that of the I-N_2 interface to be discussed later. The marked curves represent $\Delta_2(z)$ (thick rods), the unmarked ones $\Delta_1(z)$ (thin rods). Figure 4 reveals that $|\Delta_\sigma(z)|<0.017$ in the I-N_1 interface, and $|\Delta_\sigma(z)|<4.0\times10^{-4}$ in the N_1-N_2 interface. Such small biaxialities indicate that the expansion of Eq. (8), truncated at $M=1$, is accurate for calculating $\Delta_\sigma(z)$, while a truncation at $M=0$ yields accurate tensions and density profiles. In fact, we checked that the difference between the tensions based on uniaxial ($M=0$) and biaxial ($M=1$) profiles falls within the numerical accuracy, i.e., less than 1%. Our numerical data for the I-N_1 interface is consistent with that of Refs. [27,28]. Even though the magnitude of $\Delta_\sigma(z)$ is small, it is interesting to consider the structure of the profiles in some more detail. The first observation we make is that $\Delta_\sigma(z)>0$ (<0) at the isotropic (nematic) side of the I-N_1 interface for both species $\sigma=1,2$. This indicates that rods at the I side of the interface have a (small) preference for splay in the XY plane, whereas those at the N_1 side tend to ''stick'' through the interface (into the I side). A similar effect exists in the N_1-N_2 interface, but now both species have an opposite tendency (see inset): the thin rods splay in the XY plane at the N_1 side, whereas the thick ones ''stick'' through, and vice versa at the N_2 side. Recall, however, that these effects are small.

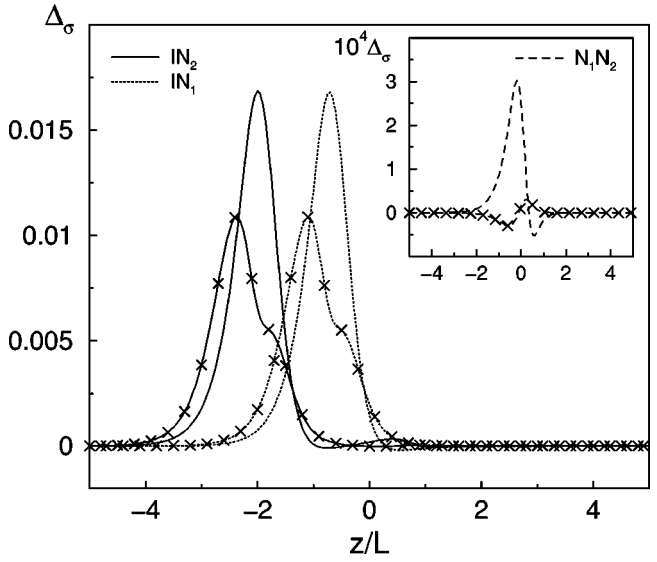

FIG. 4. Biaxiality profiles $\Delta_\sigma(z)$ of the thin (without symbols) and thick (marked by $\times$) rods in the I-N_1 and I-N_2 (at undersaturation $\epsilon=5\times10^{-4}$) interfaces for diameter ratio $d=4.0$. The inset shows the same quantity for the N_1-N_2 interface.

B. The I-N_2 interfaces

The I-N_2 interfaces exist, for $d>3.8$, in a pressure regime $p_{thick}<p<p_t$. The properties of the I-N_2 interfaces depend strongly on the pressure difference with the triple-point (I-N_1-N_2 phase coexistence). The surface tension of the I-N_2 interface shows a nonmonotonic dependence on the bulk pressure p. It develops a maximum, which is several times larger than a linear interpolation between the tension of the two pure systems, as shown in Fig. 5. It turns out that the nonmonotonic character of $\gamma_{I\text{-}N_2}(p)$ is related to the fractionation at the I-N_2 coexistence, i.e., a larger composition change through the interface leads to a larger interfacial tension. However, the surface tension which corresponds to the pressure of maximal bulk fractionation (indicated by the dashed line in Fig. 5) is lower than the maximum of $\gamma_{I\text{-}N_2}(p)$. The maximal interface stiffness grows with species diameter ratio d as the composition difference between I and N_2 phases increases (see Fig. 1). We have also compared the maximal surface tensions for different orientations of the director ($\hat{\boldsymbol{n}}\perp\hat{\boldsymbol{z}}$ and $\hat{\boldsymbol{n}}\|\hat{\boldsymbol{z}}$) in several thin-thick mixtures and found the geometry $\hat{\boldsymbol{n}}\perp\hat{\boldsymbol{z}}$ to be thermodynamically stable, i.e., $\gamma_{\hat{\boldsymbol{n}}\perp\hat{\boldsymbol{z}}}<\gamma_{\hat{\boldsymbol{n}}\|\hat{\boldsymbol{z}}}$ by at least a factor of two.

The relatively large surface tension of a mixture of rods compared to that of the pure systems of its components may well be an explanation for the relatively large tensions that

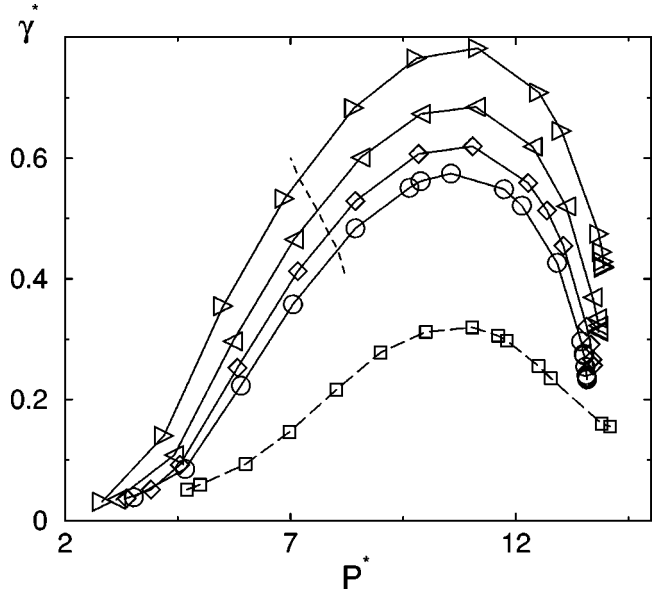

FIG. 5. Dimensionless surface tension $\gamma^*_{I\text{-}N_2}=\beta\gamma_{I\text{-}N_2}/LD_1$ at I-N_2 interfaces as a function of dimensionless pressure $p^*=\beta pL^2D_1(\pi/4)$ for different diameter ratio $d=4.0$ (○), 4.2 (◇), 4.5 (◁), 5.0 (▷) of thin-thick mixtures. The dashed line indicates the pressure of maximum fractionation. The data for $d=3.0$ (□) are included for comparison (from Ref. [28]).

were measured in suspensions of cellulose [35], which are known to be very polydisperse. This remains to be investigated in detail, however.

The dimensionless undersaturation $\epsilon=1-p/p_t$ is a convenient measure of the pressure difference with the triple point. For $0.01<\epsilon<0.5$ the profiles of the order parameters $S_\sigma(z)$ and the density of the thick component $n_2(z)$ are smooth and monotonic, whereas $n_1(z)$ shows an accumulation of thin rods at the isotropic side of the interface. This effect becomes more pronounced for small undersaturation, i.e., $\epsilon\to 0$, when a film of the nematic phase N_1 appears in the I-N_2 interface. Note that the N_1 phase is a metastable bulk phase for any $\epsilon>0$, so the film thickness is finite. For $d=4.0$ several profiles $n_1(z)$ and $n_2(z)$ for different values of ϵ are presented in Fig. 6, which clearly shows the film formation when $\epsilon\to 0$. The asymptotic densities at $z\to\pm\infty$ are those of the coexisting I and N_2 bulk phases (at the corresponding ϵ). Using translational invariance of the interface between the bulk phases, we have shifted the profiles with respect to each other such that their I-N_1 interfaces coincide. This shows that the local density of thin (thick) rods in the growing film remains constant, and exactly corresponds to the thin (thick) -rod density of the bulk triple-point phase N_1 (indicated by the dashed lines in Fig. 6). The same identification can be made for all d (or l for long-short mixtures) as well as for the order parameter profiles $S_\sigma(z)$.

The biaxiality of the I-N_2 interface was found to be small. A typical profile for thin-thick binary mixture with $d=4.0$ at $\epsilon=5\times10^{-4}$ is presented in Fig. 4. The I-N_2 biaxiality profile can be considered as a composition of the (earlier discussed) I-N_1 and N_1-N_2 profiles which is expected as the thickness of the wetting N_1 film is larger than L.

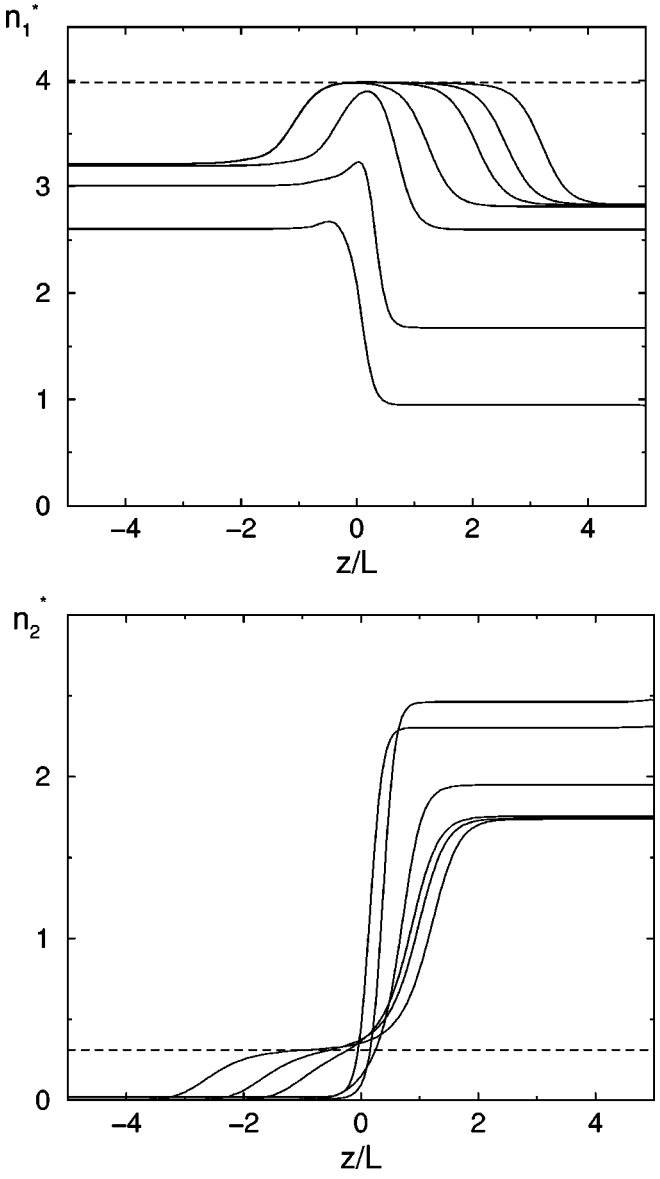

FIG. 6. Density profiles of the thin rods $n_1^*(z)$ (a) and the thick rods $n_2^*(z)$ (b) in the I-N_2 interface for diameter ratio $d=4.0$ at triple-point undersaturations $\epsilon=1-p/p_t=0.29$, 0.1, 0.01, 5×10^{-4}, 1.3×10^{-4}, 2.5×10^{-5}. The bulk I-N_2 phase is at $z\to-\infty/\infty$. The dashed lines $n_1^*=3.977$ and $n_2^*=0.312$ represent the bulk density of thin (thick) rods in the triple-point N_1 phase. These profiles indicate the formation of a wetting N_1 film in the I-N_2 interface.

For all explored mixtures the thickness of the interface t/L (or the adsorption) was found to diverge logarithmically with $\epsilon\to 0$ as shown in Fig. 7. For short-ranged interactions one expects, on the basis of mean-field theory [33], that

$$t=-\xi\ln(\epsilon)+C, \tag{11}$$

where C is an irrelevant constant offset, and ξ is the correlation length of the wetting film. This implies that the bulk correlation length ξ_{N_1} of the wetting N_1 phase should follow from the slope of the logarithmic growth of t/L in Fig. 7.

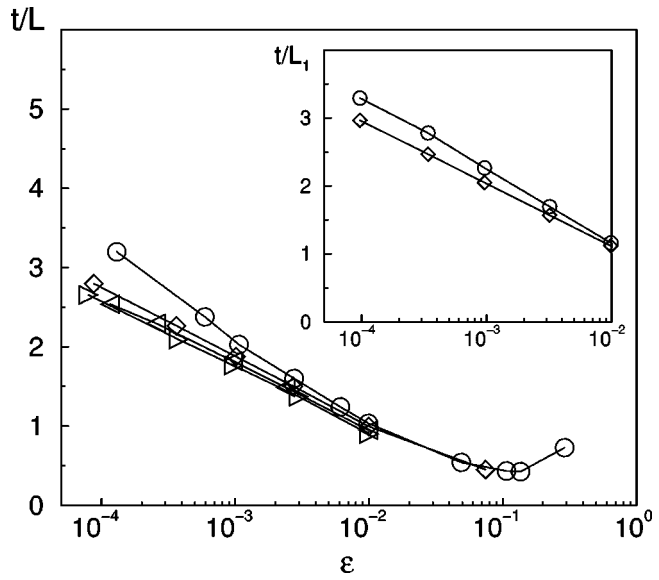

FIG. 7. Thickness t/L as a function of the undersaturation $\epsilon = 1 - p/p_t$ from the triple-point pressure p_t for diameter ratios $d = 4.0$ (○), 4.2 (◇), 4.5 (◁), 5.0 (▷) of thin-thick mixtures. The inset shows the film thickness t/L_1 for long-short mixtures with length ratio $l = 3.0$ (○), 3.1 (◇).

The asterisks (*) in Fig. 8 show the resulting values of ξ_{N_1} as a function of d. These can be compared to the correlation length that one can extract from the asymptotic decay of the one-particle distributions $\rho_\sigma(z, \hat{\boldsymbol{\omega}})$ of the I-N_1 interface into the bulk N_1 phase. This decay can best be analyzed in terms

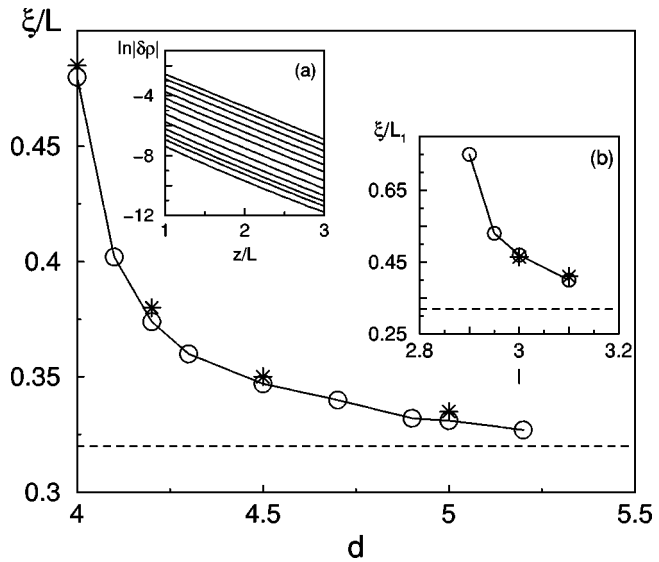

FIG. 8. Correlation length for rods in the triple-point N_1 phase of thin-thick mixtures as a function of diameter ratio d, determined from adsorption (*) analysis [Eq. (11)] and from density asymptotics (○) [Eq. (12)]. Inset (a) shows $\ln|\delta\rho(z,\theta)|$ for several values of θ at the N_1 side of the I-N_1 interface for $d = 4.0$. Inset (b) displays the correlation length (in units of length of short rods L_1) for long-short mixtures as a function of length ratio l. The dashed lines indicate the correlation length for rods in the N phase of the monodisperse hard-rod fluid.

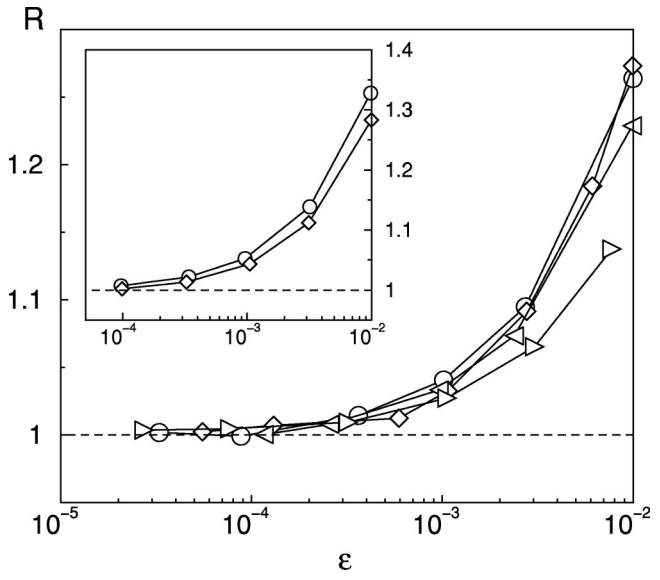

FIG. 9. Surface tension ratio R [see Eq. (13)] as a function of the triple-point undersaturation ϵ for diameter ratio $d = 4.0$ (○), 4.2 (◇), 4.5 (◁), 5.0 (▷). The inset shows the same quantity for long-short mixtures $l = 3.0$ (○), 3.1(◇).

of the deviation from the N_1 bulk density $\delta\rho_\sigma(z, \hat{\boldsymbol{\omega}}) = \rho_\sigma(z, \hat{\boldsymbol{\omega}}) - \rho_\sigma^{N_1}(\hat{\boldsymbol{\omega}})$, which we find to decay as

$$\delta\rho_\sigma(z, \hat{\boldsymbol{\omega}}) = A_\sigma(\hat{\boldsymbol{\omega}}) \exp(-z/\xi_{N_1}), \quad z \to \infty, \tag{12}$$

where the only species and orientation dependence is in the decay amplitude $A_\sigma(\hat{\boldsymbol{\omega}})$, i.e., the decay (correlation) length ξ is one and the same for all species and orientations. Such a "decay law," with a single correlation length, is well-known in mixtures of simple liquids [36]. The form (12) is illustrated for $d = 4.0$ at $p = p_t$ in the inset (a) of Fig. 8, where all curves (representing different θ's) are parallel on a logarithmic scale. The correlation length follows from the (common) slope of these curves, and is marked by (○) in the main figure. The agreement with the values of $\xi_{I\text{-}N_1}$ obtained from the logarithmic growth of the interface thickness is clearly good. The inset (b) of Fig. 8 shows the similar dependence of the bulk correlation length of triple-point N_1 phase in the case of long-short mixtures, i.e., as a function of rods length ratio l, using the same symbols.

In order to verify the thermodynamic condition of complete wetting, $\gamma_{I\text{-}N_2} = \gamma_{I\text{-}N_1} + \gamma_{N_1\text{-}N_2}$ at the triple-point pressure $p = p_t$, we determine the ratio of surface tensions

$$R(\epsilon) = \frac{\gamma_{I\text{-}N_2}(\epsilon)}{\lim_{p \downarrow p_t} (\gamma_{I\text{-}N_1} + \gamma_{N_1\text{-}N_2})}, \tag{13}$$

shown in Fig. 9. For all diameter ratios d considered here $\lim_{\epsilon \to 0} R(\epsilon) = 1$, which implies a vanishing contact angle. This constitutes the thermodynamic proof of complete triple

point wetting in all thin-thick hard-rod mixtures with $d \geq 4$. For mixtures of long and short rods the behavior of $R(\epsilon)$ is the same, as shown in the inset of Fig. 9. A mean-field analysis of the asymptotic behavior of the surface tension ($\epsilon \to 0$) in the case of complete wetting shows that [33]

$$R(\epsilon) - 1 \sim \epsilon^{2-\alpha} \tag{14}$$

with the critical exponent $\alpha = 1$. Analysis of our results in Fig. 9 gives $\alpha = 1.00 \pm 0.05$ which can be considered as a rough consistency test of our mean-field calculations.

V. SUMMARY AND DISCUSSION

We have studied free interfaces of binary mixtures of hard rods of either different diameters or different lengths within Onsager's second virial functional. On the basis of a vanishingly small wetting parameter, which implies that capillary fluctuations are not important, we argued that this mean-field functional provides a realistic description of isotropic-nematic interfaces of long hard rods. We focused on diameter ratios $d > 3.8$ (and length ratios $l > 3.0$), for which the bulk phase diagram exhibits an I-N_1-N_2 triple point, and restricted attention to the case where $\hat{\boldsymbol{n}} \perp \hat{\boldsymbol{z}}$, with $\hat{\boldsymbol{n}}$ the bulk nematic director and $\hat{\boldsymbol{z}}$ the interface normal. This is the thermodynamically most favorable geometry.

We have determined the behavior of the surface tensions of I-N_1, N_1-N_2 and I-N_2 interfaces between coexisting isotropic and nematic phases as a function of the bulk pressure and/or the diameter ratio d (length ratio l, respectively). The tension $\gamma_{I\text{-}N_1}$ is always very close to the tension of the pure fluid of thin (or short) rods, and $\gamma_{N_1\text{-}N_2}$ varies from zero at the consolute N_1-N_2 point to values as large as $\gamma_{I\text{-}N_1}$ at the triple point for $d \simeq 4-5$. The thickness of the I-N_1 and N_1-N_2 interfaces are always of the order of the lengths of the rods, except close to the N_1-N_2 consolute point, of course. The surface tension $\gamma_{I\text{-}N_2}$ is found to change nonmonotonically with pressure, exhibiting a maximum close to (but not at) that pressure where the bulk fractionation is maximal. This maximum surface tension is considerably larger than that of the pure systems of the components, typically by a factor of order 3–5, not unlike the findings of Ref. [28], where the case $d = 3$ (without any triple point) was studied. The biaxiality was found to be very small in all cases, similar to the findings in Refs. [27,28] for the one-component case. Perhaps our most interesting finding is the phenomenon of complete triple-point wetting of the I-N_2 interface by an N_1 film. The thickness of this film is found to diverge as $-\xi \ln(1 - p/p_t)$ when $p \to p_t$, with ξ the correlation length of the bulk N_1 phase, p_t the triple-point pressure, and $p < p_t$ the pressure. The triple-point wetting phenomenon is confirmed by the numerical value of the surface tensions, which satisfy $\lim_{p \uparrow p_t} \gamma_{I\text{-}N_2}(p) = \gamma_{I\text{-}N_1}(p_t) + \gamma_{N_1\text{-}N_2}(p_t)$. Such a complete wetting scenario was found for all diameter ratios $3.9 < d < 5.2$ and length ratios $2.9 < l < 3.1$ studied here. We expect that this finding will also hold for more extreme ratios $d > 5.2$ and $l > 3.1$, which are more difficult to analyze numerically because of the pronounced nematic ordering of the triple-point N_2 phase.

The predicted phenomenon of triple-point wetting may well be observable in the experimental system of bare and PEG-coated fd virus particles [23] mentioned in the Introduction. We hope that this work stimulates further experimental activities in this direction.

Another interesting direction for future theoretical work would be to consider isotropic-nematic interfaces of polydisperse mixtures, e.g., extending the theory for bulk systems developed in Ref. [37]. For suspensions of length-polydisperse cellulose experimental measurements of the surface tension have been performed [35], and show that the surface tension is much larger than that of a pure system of rods. It is tentative to speculate that the fractionation effect that is also present in binary systems may explain this increase of the tension. We hope to address this question in future work.

ACKNOWLEDGMENTS

It is a pleasure to thank Marjolein Dijkstra, Henk Lekkerkerker, and Seth Fraden for stimulating discussions, and Seth Fraden and Kirstin Purdy for sharing unpublished experimental results with us. This work is part of the research program of the Stichting voor Fundamenteel Onderzoek der Materie (FOM), which is financially supported by the Nederlandse organisatie voor Wetenschappelijk Onderzoek (NWO).

APPENDIX

In terms of $A = \frac{1}{2}\max(L_\sigma \hat{\boldsymbol{\omega}} \cdot \hat{\boldsymbol{z}}, L_{\sigma'} \hat{\boldsymbol{\omega}}' \cdot \hat{\boldsymbol{z}})$, $B = \frac{1}{2}\min(L_\sigma \hat{\boldsymbol{\omega}} \cdot \hat{\boldsymbol{z}}, L_{\sigma'} \hat{\boldsymbol{\omega}}' \cdot \hat{\boldsymbol{z}})$ and the excluded volume $E_{\sigma\sigma'} = L_\sigma L_{\sigma'} (D_\sigma + D_{\sigma'}) |\sin(\arccos(\hat{\boldsymbol{\omega}} \cdot \hat{\boldsymbol{\omega}}'))|$, the results of Ref. [25] reduce for $D_\sigma / L_\sigma \to 0$ to the following expression for the ''excluded slab'' used in Eq. (7):

$$\mathcal{K}_{\sigma\sigma'}(|z|, \hat{\boldsymbol{\omega}}, \hat{\boldsymbol{\omega}}') = \begin{cases} 0, & |z| > |A| + |B|, \\ \dfrac{E_{\sigma\sigma'}(\hat{\boldsymbol{\omega}}, \hat{\boldsymbol{\omega}}')}{4|AB|}(|A| + |B| - |z|), & |A| - |B| \leq |z| \leq |A| + |B|, \\ \dfrac{E(\hat{\boldsymbol{\omega}}, \hat{\boldsymbol{\omega}}')}{2|A|}, & |z| \leq |(|A| - |B|)|. \end{cases}$$

[1] G.J. Vroege and H.N.W. Lekkerkerker, Rep. Prog. Phys. **55**, 1241 (1992).
[2] M.P. Allen, G.T. Evans, D. Frenkel, and B.M. Mulder, Adv. Chem. Phys. **86**, 1 (1993).
[3] S. Fraden, in *Observation, Prediction and Simulation of Phase Transitions in Complex Fluids*, edited by M. Baus *et al.* (Kluwer, Dordrecht, 1995), p. 113.
[4] H. Zocher, Z. Anorg. Chem. **147**, 91 (1925).
[5] F.C. Bawden, N.W. Pirie, J.D. Bernal, and I. Fankuchen, Nature (London) **138**, 1051 (1936).
[6] L. Onsager, Ann. N.Y. Acad. Sci. **51**, 627 (1949).
[7] Z. Dogic and S. Fraden, Phys. Rev. Lett. **78**, 2417 (1997).
[8] X. Wen, R.B. Meyer, and D.L.D. Caspar, Phys. Rev. Lett. **63**, 2760 (1989).
[9] P. Bolhuis and D. Frenkel, J. Chem. Phys. **106**, 666 (1997).
[10] J.A.C. Veerman and D. Frenkel, Phys. Rev. A **41**, 3237 (1990).
[11] B. Mulder, Phys. Rev. A **35**, 3095 (1987).
[12] A. Poniewierski and R. Holyst, Phys. Rev. Lett. **61**, 2461 (1988).
[13] A.M. Somoza and P. Tarazona, Phys. Rev. Lett. **61**, 2566 (1988); Phys. Rev. A **41**, 965 (1990).
[14] H.N.W. Lekkerkerker, Ph. Coulon, R. Van Der Haegen, and R. Deblieck, J. Chem. Phys. **80**, 3427 (1984).
[15] Th. Odijk and H.N.W. Lekkerkerker, J. Phys. Chem. **89**, 1272 (1985).
[16] T.M. Birshtein, B.I. Kolegov, and V.A. Pryamitsyn, Polym. Sci. U.S.S.R. **30**, 316 (1988).
[17] G.J. Vroege and H.N.W. Lekkerkerker, J. Phys. Chem. **97**, 3601 (1993).
[18] R. van Roij and B. Mulder, Phys. Rev. E **54**, 6430 (1996).
[19] R. van Roij and B. Mulder, J. Chem. Phys. **105**, 11237 (1996); **109**, 1584 (1998).
[20] M. Dijkstra and R. van Roij, Phys. Rev. E **56**, 5594 (1997).
[21] R. van Roij, B. Mulder, and M. Dijkstra, Physica A **261**, 374 (1998).
[22] R. Sear and G. Jackson, J. Chem. Phys. **103**, 8684 (1995).
[23] K. Purdy and S. Fraden (private communication).
[24] Z.Y. Chen and J. Noolandi, Phys. Rev. A **45**, 2389 (1992).
[25] A. Poniewierski and R. Holyst, Phys. Rev. A **38**, 1527 (1988).
[26] B.G. Moore and W.E. McMullen, Phys. Rev. A **42**, 6042 (1990).
[27] Z.Y. Chen, Phys. Rev. E **47**, 3765 (1993).
[28] K. Shundyak and R. van Roij, J. Phys.: Condens. Matter **13**, 4789 (2001).
[29] A.J. McDonald, M.P. Allen, and F. Schmid, Phys. Rev. E **63**, 010701 (2001).
[30] K. Shundyak and R. van Roij, Phys. Rev. Lett. **88**, 205501 (2002).
[31] R. Evans, Adv. Phys. **28**, 143 (1979).
[32] J. S. Rowlinson and B. Widom, *Molecular Theory of Capillarity* (Clarendon, Oxford, 1982).
[33] M. Schick, in *Liquids at Interfaces*, edited by J. Charvolin *et al.* (Elsevier, Amsterdam, 1990), p. 415.
[34] P.C. Hemmer, Mol. Phys. **96**, 1153 (1999).
[35] W. Chen and D.G. Gray, Langmuir **18**, 633 (2002).
[36] R. Evans, R.J.F. Leote de Carvalho, J.R. Henderson, and D.C. Hoyle, J. Chem. Phys. **100**, 591 (1994).
[37] P. Sollich, J. Phys.: Condens. Matter **14**, R79 (2002).